2024 IEEE International Conference on Robotics and Automation (ICRA 2024)
May 13-17, 2024. Yokohama, Japan

Model Design and Concept of Operations of Standard Interface for On-orbit Construction

Jingdong Zhao, Zirui Wang, Ziyi Liu, Liangliang Zhao*, Qifan Duan, Hong Liu

***Abstract*— The construction of large-scale space facilities requires the use of on-orbit construction technology. However, several of its key components, such as standard interface design, compliant control methods, and path planning for multi-branch robots, still need improvement before practical application. This paper presents a comprehensive solution for on-orbit construction tasks, encompassing a novel standard interface, docking control method, and path planning method for space multi-branch robots. Firstly, a novel standard interface is introduced, which features multiple mating modes and a lightweight design. Additionally, a compliant docking method is provided to generate lower contact forces along the Z-direction. Furthermore, for four-armed space robots, a hierarchical planning method is proposed, which innovates in environment map construction and locomotion planning. Specifically, the closed-form Minkowski sum method is employed to solve the robot's free space, and a concise locomotion method is elucidated based on transition support points. Finally, simulations and experiments are conducted.**

***Index Terms*— On-orbit construction, space robot, standard interface, docking control, path planning.**

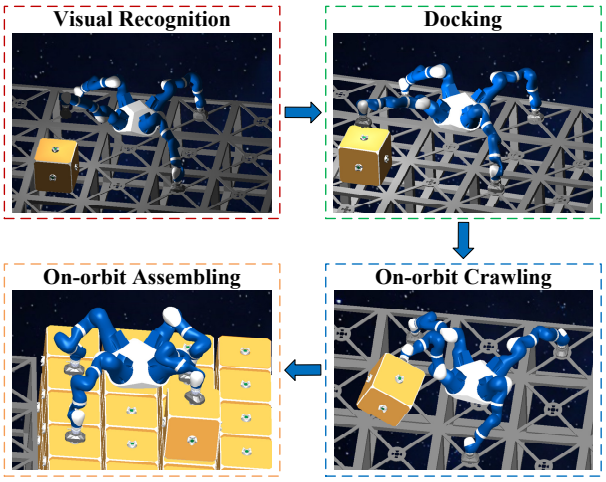

Fig. 1. Illustration of an on-orbit construction task. First, the robot recognizes the module in a dark environment. Then, it captures the module and crawls on discrete standard interfaces. Finally, the module is assembled.

I. Introduction

With the continuous advancement of space science and technology, there is a growing demand for the construction of large space telescopes [1], [2], space solar power stations [3], [4], and space antennas [5]. In 2016, the California Institute of Technology introduced the RAMST project, aimed at constructing an exceptionally large space telescope with a 100-meter diameter, consisting of over 300 modules [6]. However, due to constraints related to mass, volume, and payload capacity associated with traditional rocket launch methods, the construction of these large-scale space facilities necessitates the on-orbit construction technology [7].

In many concepts, multi-branch relocatable space robots are the ideal candidates for on-orbit assembly tasks [8]–[10]. As illustrated in Fig. 1, these robots are expected to perform tasks such as recognizing the pose of modules, capturing them, transporting them, and subsequently assembling these modules on-orbit. To address the increasing demand for component connections in the scenarios mentioned above, various standard interfaces have been developed. However, the standard interfaces can be optimized specifically for the on-orbit crawling task. In some prototypes of multi-branch space robots, an impedance control method is employed to reduce the contact force during module capture [11], [12]. However, it is important to note that the accuracy of the dynamics model significantly influences the output due to its inherent force-control loop. When it comes to the challenge of multi-branch space robots crawling on discrete standard interfaces, there is still a lack of an intuitive and concise method for locomotion.

In this paper, a novel standard interface, as well as a docking control method and path planning method, are presented to address those limitations. The main contributions are outlined as follows:

1) A novel standard interface, characterized by multiple mating modes and a lightweight design, is introduced. For four-guided androgynous form-fit geometry, the theoretical value of misalignment tolerance is derived, which is in agreement with the experimental results.
2) A compliant docking control method, based on a six-dimensional force sensor, is provided. It will be demonstrated that lower contact force in the Z-direction is achieved when compared to the impedance control method utilized within the KUKA manipulator.
3) A hierarchical path planning method, which innovates in locomotion planning, is elaborated upon. For locomotion planning on planar trusses, a novel method based on transition support points is proposed, which is both easily comprehensible and implementable.

Research supported by the National Natural Science Foundation of China (Grant 92148203), Self-Planned Task (NO.SKLRS202201A01) of State Key Laboratory of Robotics and System (HIT) and National Key Laboratory of Aerospace Flight Dynamics Foundation (NO.XTB6142210210303).

Jingdong Zhao, Zirui Wang, Liangliang Zhao, Hong Liu are with the State Key Laboratory of Robotics and System, Harbin Institute of Technology, Harbin 150080, China. Ziyi Liu is with the Chang Guang Satellite Technology Co., Ltd., Changchun 130000, China. Qifan Duan is with the Beijing Honor Device Co., Ltd., Beijing 100095, China.

*Corresponding author: Liangliang Zhao (zhaoliangliang@hit.edu.cn).

The remainder of this paper is organized as follows. Section II provides a brief overview of previous research. Section III delves into the novel standard interface, offering a comprehensive introduction of its components and a theoretical analysis of misalignment tolerance. Section IV is dedicated to the on-orbit assembly task, which is divided into three key components: "visual recognition", "compliant docking", and "on-orbit crawling". Simulations and experiments are conducted in Section V. Section VI summarizes the paper.

II. Related Works

To address the needs of modular structure on-orbit assembly, various standard interfaces have been developed worldwide. In 2017, iBOSS introduced the Intelligent Space System Interface (ISSI), which encompassed mechanical, electrical, data, and thermal coupling functions [13], [14]. Modular design enabled it to meet a broad range of requirements simply by adding add-on modules. The standard HOTDOCK interface, designed by Belgian Space Applications Services in 2018, featured mechanical connection, data communication, power transmission, and heat transfer capabilities [15]. This interface utilized a four-guided androgynous docking surface, offering substantial misalignment tolerance and docking flexibility. The Standard Interface for Robotic Manipulation (SIROM), developed by SENER Aeroespacial in 2018, extended its functionalities to include fluid transport interface capabilities [16]. In 2021, Altius Space Machines presented the ESCHER interface for autonomous in-space or lunar surface assembly [17]. The unique EPM latching technology ensured high reliability during the assembly process. In 2022, GITAI produced the grapple end-effector for its inchworm robot [18]. Equipped with cameras and LEDs, it allowed the robot to perform a wide variety of general-purpose tasks, like inchworm crawling and tool changing. Nevertheless, for the on-orbit crawling task which doesn't necessitate electrical connection, the standard interfaces can be further optimized.

To prevent structural damage caused by contact forces during the docking process, compliant control methods are commonly employed, which include impedance control, admittance control, and hybrid position/force control. Hogan initially proposed impedance control in 1985, comprising both an internal force control link and an external impedance control link [19]. In contrast, position-based admittance control consists of an internal position control link and an external admittance control link [20]. Hybrid position/force control is a comprehensive approach that incorporates both a position control loop and a force control loop [21]. It finds widespread application in scenarios requiring control over both position and contact forces, such as robot grinding.

The challenge of multi-arm space robots crawling on discontinuous terrain remains an emerging research area. Yue et al. introduced a systematic hierarchical path planning framework that encompasses global trajectory planning, local behavior planning, and arm motion planning [22]. MOSAR-WM utilized a state transition graph to plan locomotion and generated joint trajectories through a combination of the RRTConnect algorithm and the lines-and-parabolas method [23]. Jiang et al. presented an autonomous planning method founded on dynamic potential fields, enabling the robot to adjust its gait through a hybrid event-time trigger mechanism [24]. When dealing with planar conditions, a more intuitive and concise locomotion planning method based on transition support points is proposed.

(a) (b) (c)

Fig. 2. Three versions of the standard interface. (a) Active interface. (b) Passive interface. (c) Lightweight interface.

TABLE I
SUPPORTED FEATURE IN EACH VERSION

Name	Mechanical Connection	Power/Data Connection	Visual	Application
Active	✓	✓	✓	docking crawling (active side)
Passive	✓	✓		docking (passive side)
Lightweight	✓			crawling (passive side)

III. Standard Interface Design

The standard interface comprises five key modules: a docking module, a locking module, an electrical connection module, a vision module, and a control module. The docking module serves to rectify docking errors and facilitate load transfer. Upon successful docking, the mechanical connection is completed by the locking module, and electrical connectivity is established through POGO pins/pads. The vision module plays a dual role in illuminating the dark environment and recognizing the pose of the module. The control module manages the operation of all these modules.

Three versions of the standard interface have been developed to optimize mass and cost, as shown in Fig. 2. The active interface incorporates all the aforementioned modules, while the passive interface is a simplified version with form-fit geometry and electrical connectors. The lightweight interface is a plate with specifically designed circular slots.

Featuring mechanical connection, power connection and visual recognition capabilities, the active interface can be used as a robotic end-effector, participating in the whole process of on-orbit assembly. The passive interface can be installed on payload modules, facilitating the compliant docking process of the manipulator. The lightweight interface is designed for tasks that exclusively necessitate mechanical connections without electrical connections, such as on-orbit crawling. A summary of their functions is shown in Table I.

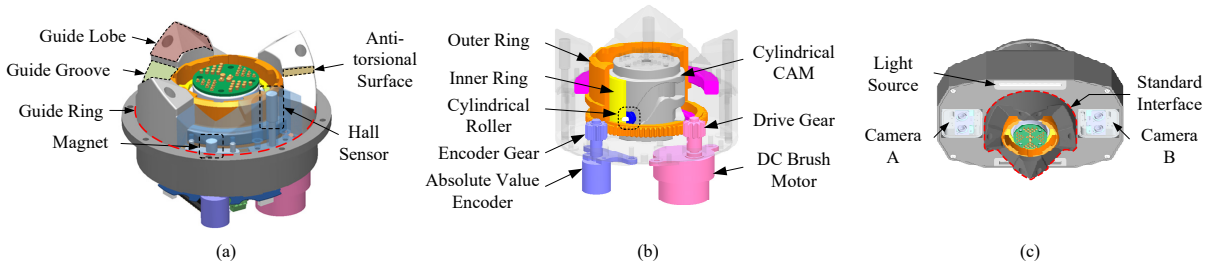

Fig. 3. Overall structure of standard interface. (a) Docking module structure. (b) Locking module structure. (c) Vision system.

A. Model Design

As illustrated in Fig. 3(a), the docking module incorporates an androgynous design with 90° rotational symmetry, comprising a guide ring, a Hall-effect sensor, and a magnet. During the docking process, the guide ring corrects position and orientation errors, while the Hall-effect sensor detects the magnetic field strength to ascertain the completion of the docking procedure. The guide ring itself consists of an anti-torsional surface, a guide lobe, and a guide groove. The anti-torsional surface is specifically designed to counteract torque around the Z-direction, while the guide lobe enables large misalignment tolerance, which will be analyzed later.

As shown in Fig. 3(b), the locking module comprises several components, including a cylindrical CAM, cylindrical roller, inner ring, outer ring, drive gear, encoder gear, DC brush motor, and an absolute value encoder. Following successful docking, the locking module is employed to constrain movement along the Z-direction on both sides and establish a stable and reliable mechanical connection. The locking module adheres to the design principles of androgyny and 90° rotational symmetry. The locking process can be broken down into three distinct steps: extraction, maintenance, and contraction. In the extraction phase, the inner lock hooks pass through the gaps between the outer lock hooks and rise above them. Subsequently, the inner lock hooks maintain a fixed height for a short time before finally descending to press on the outer lock hooks. If the active side fails, unlocking can be accomplished by reverse rotation on the passive side.

As shown in Fig. 3(c), the vision system comprises two cameras and an LED light source. Specifically, two Intel Realsense D405 cameras are positioned on either side of the standard interface, enabling the simultaneous capture of color and depth images. Additionally, a light source is installed to provide illumination in dark environments. Table II shows the comparison between our standard interface and the state-of-the-art interfaces. Our standard interface features a more compact size and smaller mass.

B. Misalignment Tolerance Analysis

The form-fit geometry is illustrated in Fig. 4(a). Let's define the following parameters: R_o as the outer radius of the guide ring, R_i as the inner radius of the guide ring, H as the height of the guide lobe, h as the width of the anti-torsional surface, β as the radial guide angle, and α as the

TABLE II
COMPARISON BETWEEN SOTA STANDARD INTERFACES AND OURS

Name	Diameter(mm) (active)	Height(mm) (active)	Mass(kg)
iSSI	143.7	54.2	1/0.65/0.2
HOTDOCK	148	70	1.55/0.5/0.25
SIROM	128	76.6	1.5
Ours	95	86.0	1/0.35/0.08

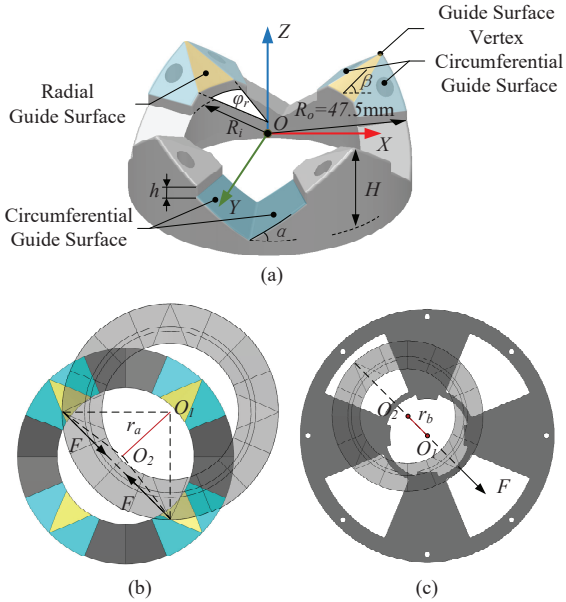

Fig. 4. Misalignment tolerance of docking module. (a) Geometric parameters. (b) Tolerance boundary of passive interface. (c) Tolerance boundary of lightweight interface.

circumferential guide angle. The circumferential guide angle can be expressed as:

$$\alpha = \arctan\left(\frac{4(H-h)}{\pi R_o}\right) \tag{1}$$

According to the direction of the contact force, the guide lobe can be classified into two circumferential guide surfaces and one radial guide surface. When the guide surface vertex of the mating interface makes contact with the circumferential guide surfaces, the contact force pushes the mating surface towards the center. Conversely, if it makes contact with the radial guide surface, the contact force becomes

TABLE III
GEOMETRIC PARAMETERS OF DOCKING MODULE

Parameters	Value	Parameters	Value
R_o/mm	47.5	R_i/mm	30
H/mm	30	h/mm	4
β/°	30	α/°	34.88
r_a/mm	27.89	r_b/mm	17.5

orthogonal to the position vector between the centers of the two interfaces. As shown in Fig. 4(b), if two adjacent guide surface vertices both contact the radial guide surface of the opposite side, their contact forces will offset, resulting in a failed docking attempt. Based on these analyses, the approximate inscribed circle radius of the misalignment tolerance area can be described as:

$$r_a = R_o \cos(\pi/4) - \frac{R_i \sin(\varphi_r/2)\left[R_o - R_o \sin(\pi/4)\right]}{R_o - R_i \cos(\varphi_r/2)} \quad (2)$$

where φ_r is the central angle of the radial guide surface, which can be represented as:

$$\varphi_r = \frac{\pi}{4} - \frac{H - 2\tan\beta(R_o - R_i) - h}{\tan\alpha R_i} \quad (3)$$

As illustrated in Fig. 4(c), when it comes to the lightweight interface, the essential requirement for successful docking is: the axial projections of all four guide surface vertices on the active interface must lie within the circular slot on the lightweight interface. Consequently, the approximate inscribed circle radius of the axial misalignment tolerance area can be described as:

$$r_b = R_o - R_i \quad (4)$$

The geometric parameters of the standard interface are provided in Table III. Among these parameters, the outer radius R_o, inner radius R_i, height H, anti-torsional surface width h, and radial guide angle β are selected manually based on structural constraints. The circumferential guide angle α, as well as the misalignment area radius r_a, r_b, are calculated using the aforementioned formulas.

IV. CONCEPT OF OPERATIONS

The on-orbit assembly can be divided into three subtasks: visual recognition, compliant docking and on-orbit crawling.

A. Visual Recognition

The visual recognition working scenario is shown in Fig. 5. The goal of visual recognition is to determine the homogeneous transformation matrix T_G^W between the module coordinate G and the world coordinate W, which can be expressed by the homogeneous transformation equation:

$$T_G^W = T_E^W \cdot T_{C_1}^E \cdot T_G^{C_1} = T_E^W \cdot T_{C_2}^E \cdot T_G^{C_2} \quad (5)$$

where E denotes the end effector coordinate, C_1 and C_2 represent the camera coordinates. T_E^W can be acquired from

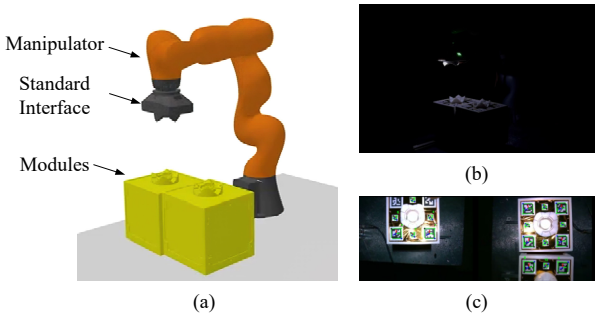

Fig. 5. Working scenario of visual recognition. (a) The experimental setup includes a manipulator with a standard interface and modules. (b) In a dark environment, the LED light source is activated, providing illumination. (c) Using the local cameras integrated into the standard interface, Aruco markers on the modules are detected, and their poses are recognized.

the manipulator, and $T_{C_1}^E$ and $T_{C_2}^E$ remain constant. Solving for $T_G^{C_1}$ and $T_G^{C_2}$ can be simplified to the PnP problem, which can be readily implemented using the OpenCV library.

B. Compliant Docking

As shown in Fig. 6, the compliant docking control system comprises both an inner position control loop and an outer compliant control loop. The process initiates with the acquisition of the measured contact force F_s via a six-dimensional force sensor. However, owing to gravitational interference in ground test and sensor zero shift, additional processing is required to derive the actual contact force F_r. Building upon this, control is segmented into two components: motion control along the Z-direction and control for the other five motion directions, facilitated by a selection matrix denoted as S. Essentially, this selection matrix S is a diagonal matrix, with a value of 1 corresponding to movement along the Z-direction and 0 for the other five movements. In Z-direction motion control, the system first calculates the tracking error between the contact force F_r and the expected contact force F_d. This error is then transformed into a pose correction Δx_1 through the motion coefficient matrix K_f. For the remaining five motion control directions, the respective contact forces are transformed into pose corrections Δx_2 by adjusting the motion coefficient matrix K_c. Ultimately, based on the pose corrections Δx_1 and Δx_2, the desired pose x_d is derived by modifying the robot's current pose, which is subsequently tracked by the internal position control loop. The docking control method can be represented as:

$$\Delta x = (F_r \cdot S - F_d) \cdot K_f + F_r \cdot (I - S) \cdot K_c \quad (6)$$

$$x_d = x + \Delta x \quad (7)$$

C. On-orbit Crawling

For a four-armed space robot, a hierarchical planning method is employed to determine a viable trajectory. The process begins with the construction of an environment map, as shown in Fig. 7. Utilizing the planar truss model, the environment map is initialized, with each support point corresponding to a grid node. To enhance search efficiency, invalid

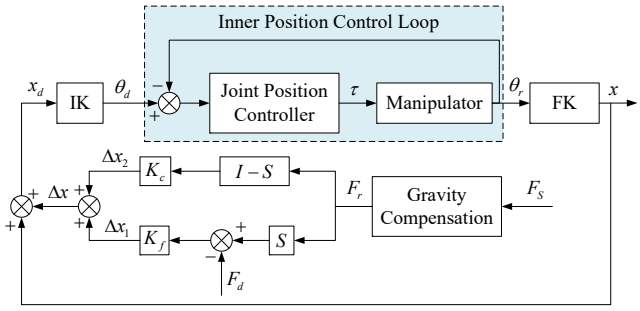

Fig. 6. The diagram of compliant docking method (ground test)

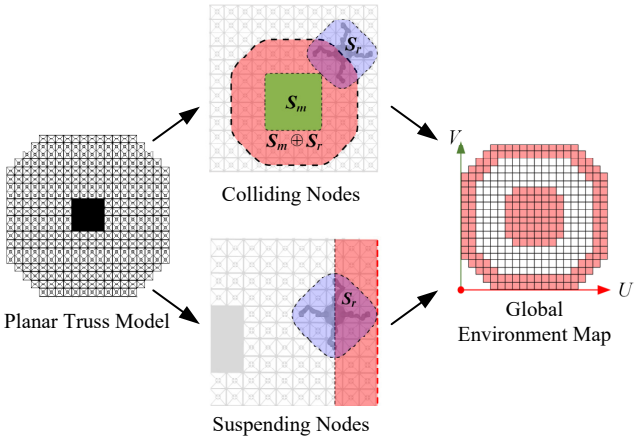

Fig. 7. Construction of environment map. First, we can initialize the grid map from planar truss model. Then, colliding nodes and suspending nodes are removed from grid map by closed-form Minkowski sum method. Finally, the global environment map is obtained.

nodes must be filtered out, including "colliding nodes" which occur when the space multi-branch robot encounters an obstruction, and "suspending nodes" which occur when any branch of the robot lacks a supporting node.

The collision problem between the robot and the module warehouse can be effectively resolved by utilizing the closed-form Minkowski sum approach between superelliptic curves [25]. Building on this, the Minkowski sum between the superelliptic envelope of the robot and that of the module warehouse is calculated, as illustrated in Fig. 7. Any node located within this Minkowski sum region is identified as invalid. A similar method is employed to determine the suspending nodes. Once these invalid nodes are removed, the environment map is completed.

Next, the A* algorithm is employed to plan a global path for the robot center. To let the robot follow the global path, a novel locomotion planning method based on transition support points is proposed. As shown in Fig. 8, for the initial state of a motion period, the support points in the working space of the manipulator are defined as the current available support points (blue). For the goal state of a motion period, the support points in the working space of the manipulator are defined as the target available support points (yellow). The transition support points are the intersection between

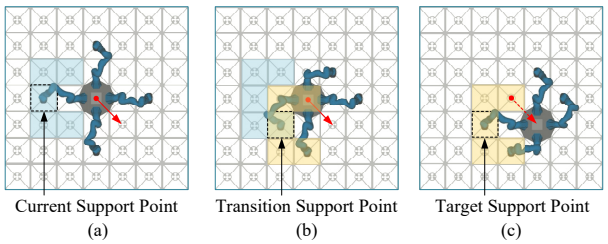

Fig. 8. The process of transfer between adjacent nodes. (a) Initial state. (b) Transition state. (c) Goal state.

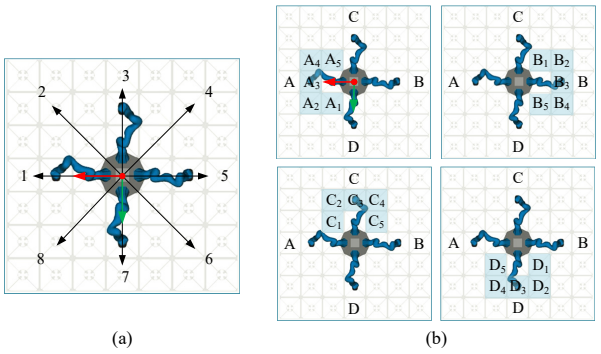

Fig. 9. Moving directions and current available support points. (a) Possible moving directions. (b) Current available support points for each branch.

TABLE IV
RESULTS OF THE TRANSITION SUPPORT POINTS

Directions	Transition support points			
	Branch A	Branch B	Branch C	Branch D
1	A_2, A_4	B_1, B_5	C_2, C_3	D_3, D_4
2	A_3	B_1	C_3	D_5
3	A_3, A_4	B_2, B_3	C_2, C_4	D_1, D_5
4	A_5	B_3	C_3	D_1
5	A_1, A_5	B_2, B_4	C_3, C_4	D_2, D_3
6	A_1	B_3	C_5	D_3
7	A_2, A_3	B_3, B_4	C_1, C_5	D_2, D_4
8	A_3	B_5	C_1	D_3

the current available support points and the target available support points. During the transition between adjacent nodes, the robot arm should move from the current support point to the transition support point, and collaborate with the robot body to reach the target support point. Consequently, determining the transition support points becomes the pivotal aspect of locomotion planning.

To clearly elaborate the algorithm, the moving directions are numbered in Fig. 9(a), and the current available support points are encoded in Fig. 9(b). The result of the transition support points is shown in Table IV. For example, if the robot plans to move left, its branch A should move to A_2 or A_4 point first, then branch B to B_1 or B_5, subsequently branches C and D. After all the branches reach their transition support points, we can let the robot center move left.

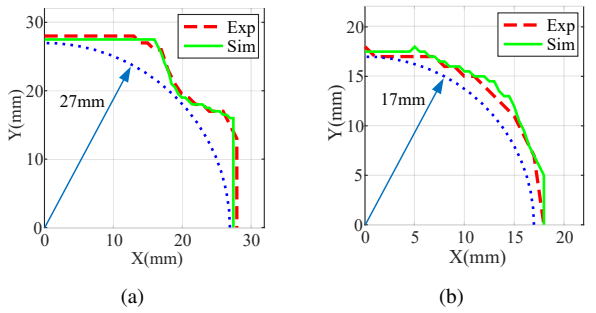

Fig. 10. Simulation and experiment result of radial misalignment tolerance. (a) Passive interface. (b) Lightweight interface.

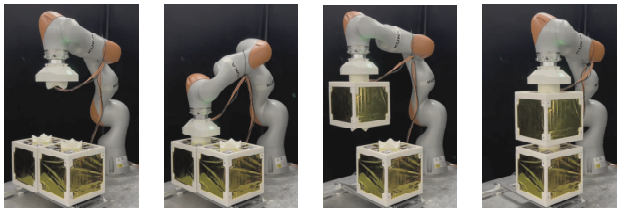

Fig. 11. Snapshots of autonomous module assembly experiment. (a) Recognize. (b) Dock. (c) Carry. (d) Assemble.

V. Simulations and Experiments

A. Misalignment Tolerance Simulation and Experiment

The docking simulation is conducted using ADAMS software. Building upon these simulation results, experiments are conducted using the KUKA iiwa LBR 14 manipulator. The manipulator is controlled by a position control method, and the payload module is fixed on a moving chassis. The outcomes are presented in Fig. 10, clearly demonstrating that the theoretical analysis, simulation, and experiment produced consistent results. Specifically, the approximate inscribed circle radius of the radial misalignment tolerance region is 27 mm on the passive interface, and 17 mm on the lightweight interface. Besides, the rotational tolerance is 12°.

B. Autonomous Module Assembly Experiment

Position-based visual servoing is implemented to guide the KUKA manipulator in autonomously assembling the payload modules. Snapshots of the experiment are displayed in Fig. 11. The error in visual recognition remains below 2 mm.

C. Compliant Docking Experiment

As shown in Fig. 12(a), experiments are conducted under the condition of a 10 mm pose error in the X-direction, employing both compliant control and impedance control methods. The results of contact forces are presented in Fig. 12(b) and (c). While the maximum contact forces along the X-direction are comparable, the compliant control method exhibits a lower maximum contact force along the Z-direction. Repeated experiments under various position and orientation error conditions consistently indicate that the compliant control method can reduce the maximum contact force along the Z-direction by approximately 20%.

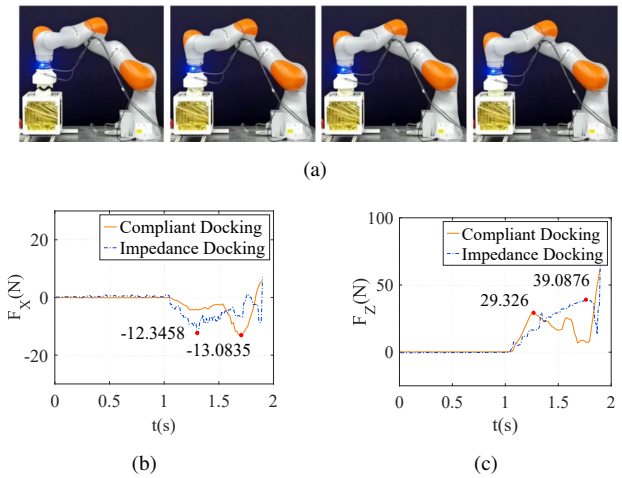

Fig. 12. Result of compliant docking experiment. (a) Snapshots. (b) Contact force along X direction. (c) Contact force along Z direction.

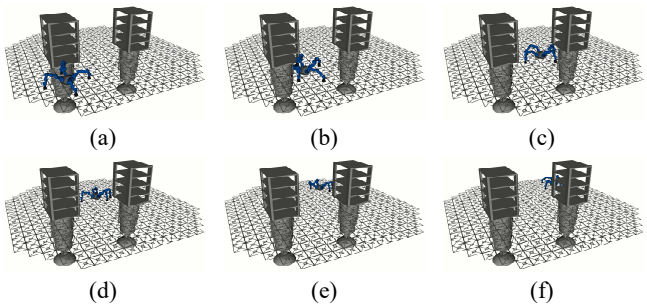

Fig. 13. Snapshots of on-orbit climbing experiment. (a) Initial position. (b)-(e) Midpoints. (f) Goal position.

D. On-orbit Crawling Simulation

Based on our hierarchical planning method, an on-orbit crawling simulation is conducted, as shown in Fig. 13. The multi-branch robot successfully avoids collision with the warehouse and reaches its intended destination.

VI. Conclusion

In this paper, a novel standard interface, as well as comprehensive solutions are provided for on-orbit assembly tasks. Initially, the structure of the standard interface is introduced, which encompasses the docking module, locking module, and vision system, with a particular highlight on lightweight interface design. Subsequently, the on-orbit assembly task is divided into three subtasks: visual recognition, compliant docking and on-orbit crawling, which are addressed separately. Finally, simulations and experiments are conducted.

In the aforementioned experiment, a proof-of-concept model is constructed to validate the operational concepts. However, the electrical connection module has not been fully implemented at this stage. Our plan is to develop a fully-functional prototype for conducting a TRL4 experiment. Furthermore, our path planning algorithm has not undergone real experimental verification, which will be supplemented after the construction of a multi-arm space robot crawling environment.

REFERENCES

[1] C. Underwood, *et al.*, "Using cubesat/micro-satellite technology to demonstrate the autonomous assembly of a reconfigurable space telescope (aarest)," *Acta Astronautica*, vol. 114, 2015.

[2] B. Baldauf, *et al.*, "Modular orbital demonstration of an evolvable space telescope (modest)," in *AIAA SPACE 2015 Conference and Exposition*, 2015.

[3] C. Yang, X. Hou, and L. Wang, "Thermal design, analysis and comparison on three concepts of space solar power satellite," *Acta Astronautica*, vol. 137, 2017.

[4] J. Mankins, N. Kaya, and M. Vasile, "Sps-alpha: the first practical solar power satellite via arbitrarily large phased array (a 2011-2012 niac project)," in *10th International Energy Conversion Engineering Conference*, 2012.

[5] P. Amaro-Seoane, *et al.*, "Laser interferometer space antenna," *arXiv preprint arXiv:1702.00786*, 2017.

[6] N. Lee, *et al.*, "Architecture for in-space robotic assembly of a modular space telescope," *Journal of Astronomical Telescopes, Instruments, and Systems*, vol. 2, 2016.

[7] Z. Xue, *et al.*, "Review of in-space assembly technologies," *Chinese Journal of Aeronautics*, vol. 34, 2021.

[8] M. Deremetz, *et al.*, "Concept of operations and preliminary design of a modular multi-arm robot using standard interconnects for on-orbit large assembly," in *72nd International Astronautical Congress (IAC)*, 2021.

[9] P. J. Staritz, *et al.*, "Skyworker: a robot for assembly, inspection and maintenance of large scale orbital facilities," in *2001 IEEE International Conference on Robotics and Automation (ICRA)*, 2001.

[10] R. P. Hoyt, *et al.*, "Spiderfab: An architecture for self-fabricating space systems," in *AIAA Space 2013 conference and exposition*, 2013.

[11] M. Deremetz, *et al.*, "Design and integration of a multi-arm installation robot demonstrator for orbital large assembly," in *73rd International Astronautical Congress (IAC)*, 2022.

[12] S. Scherzinger, *et al.*, "A walking space robot for on-orbit satellite servicing: The recobot," in *2022 IEEE 18th International Conference on Automation Science and Engineering (CASE)*, 2022.

[13] T. Schervan, *et al.*, "New horizons for exploration via flexible concepts based on building blocks using the standardized issi (intelligent space system interface) modular coupling kit by iboss," in *Global Space Exploration Conference*, 2021.

[14] J. Kreisel, T. A. Schervan, and K. U. Schroeder, "A game-changing space system interface enabling multiple modular and building block-based architectures for orbital and exploration missions," in *70th International Astronautical Congress (IAC)*, 2019.

[15] P. Letier, *et al.*, "Hotdock: Design and validation of a new generation of standard robotic interface for on-orbit servicing," in *71st International Astronautical Congress (IAC)*, 2020.

[16] M. Díaz-Carrasco Díaz, *et al.*, "Sirom electronics design: Current state and future developments," *Acta Astronautica*, vol. 202, 2023.

[17] A. S. Machines. (2021) Technologies of altius - in-space assembly. [Online]. Available: https://altius-space.com/technologies

[18] S. Nakanose and K. Nakamura-Messenger, "GITAI USA: Providing Safe and Affordable Means of Labor in Space," in *ASCEND 2023*, 2023.

[19] N. Hogan, "Impedance control: An approach to manipulation," in *1984 American control conference*, 1984.

[20] A. Calanca, R. Muradore, and P. Fiorini, "A review of algorithms for compliant control of stiff and fixed-compliance robots," *IEEE/ASME transactions on mechatronics*, vol. 21, 2015.

[21] M. Reibert and J. Craig, "Hybrid position/force control of manipulators," *ASME, J. of Dynamic Systems, Measurement, and Control*, vol. 103, 1981.

[22] C. Yue, *et al.*, "Hierarchical path planning for multi-arm spacecraft with general translational and rotational locomotion mode," *Science China Technological Sciences*, vol. 66, 2023.

[23] A. Huzynets, *et al.*, "Motion planning for relocatable robots performing on-orbit locomotion and manipulation tasks," in *73rd International Astronautical Congress (IAC)*, 2022.

[24] J. Jiang, *et al.*, "Autonomous planning of discontinuous terrain-dependent crawling for space dobby robots," *Sensors*, vol. 23, 2023.

[25] S. Ruan and G. S. Chirikjian, "Closed-form minkowski sums of convex bodies with smooth positively curved boundaries," *Computer-Aided Design*, vol. 143, 2022.